Journal of Power Sources 246 (2014) 409–416

Contents lists available at ScienceDirect

Journal of Power Sources

journal homepage: www.elsevier.com/locate/jpowsour

Nanostructuring of $SmBa_{0.5}Sr_{0.5}Co_2O_{5+\delta}$ cathodes for reduced-temperature solid oxide fuel cells

Da Han, Hao Wu, Junliang Li, Shaorong Wang*, Zhongliang Zhan*

CAS Key Laboratory of Materials for Energy Conversion, Shanghai Institute of Ceramics, Chinese Academy of Sciences (SICCAS), 1295 Dingxi Road, Shanghai 200050, China

HIGHLIGHTS

- $SmBa_{0.5}Sr_{0.5}Co_2O_{5+\delta}$/LSGM cathode of nanostructure is fabricated by impregnation method.
- The lowest ARS values of $SmBa_{0.5}Sr_{0.5}Co_2O_{5+\delta}$/LSGM cathode is 0.035 Ω cm^2 at 550 °C and 0.12 Ω cm^2 at 500 °C.
- Power densities of 1.5 W cm^{-2} at 600 °C and 0.70 W cm^{-2} at 500 °C were obtained.

ARTICLE INFO

Article history:
Received 23 May 2013
Received in revised form
26 July 2013
Accepted 29 July 2013
Available online 6 August 2013

Keywords:
Layered perovskite oxides
Cathodes
Impregnation
Reduced temperature solid oxide fuel cells

ABSTRACT

Here we report the fabrication of composite cathodes for reduced-temperature solid oxide fuel cells by impregnating aqueous solutions corresponding to $SmBa_{0.5}Sr_{0.5}Co_2O_5$ (SBSCO) into the porous $La_{0.9}Sr_{0.1}Ga_{0.8}Mg_{0.2}O_{3-\delta}$ (LSGM) backbones. Examination of X-Ray diffraction patterns indicates that phase-pure SBSCO layered perovskite oxides can be only achieved at calcination temperatures ≥900 °C. Based upon impedance measurement of symmetric cells, the SBSCO–LSGM composites calcinated at 850 °C show a trade-off between the SBSCO phase purity and catalyst size, and thereby exhibit minimal cathode polarization resistances with respect to the infiltrate calcination temperature, *e.g.*, 0.035 Ω cm^2 at 550 °C and 0.12 Ω cm^2 at 500 °C at the loadings of 21 wt%. Analysis of impedance spectra under varied oxygen partial pressures suggests that oxygen reduction reactions on the nano-scale SBSCO–LSGM composite are largely dominated by ionization of adsorbed oxygen atoms on the SBSCO surfaces. Thin LSGM electrolyte fuel cells with impregnated Ni anodes and SBSCO cathodes show high power densities of 1.5 W cm^{-2} at 600 °C and 0.70 W cm^{-2} at 500 °C.

1. Introduction

Fuel cells have been considered as one of the most important power generation technologies to efficiently convert fuels into electricity in an environmentally friendly manner. Among various types of fuel cells, solid oxide fuel cells (SOFCs) operate at elevated temperature, and exhibit some unique advantages such as high energy efficiencies, wide fuel flexibilities and rapid electrode kinetics without the use of noble metals as the catalysts [1–3]. Extensive efforts have been made to reduce the SOFC operating temperature from the conventional 700–900 °C down to 500–600 °C, which allows broad choice of the electrode and interconnecting materials, reduces the system costs and increases the performance durability [4,5]. Nevertheless, the SOFC power density would drop dramatically at low temperatures due to exponentially increased ohmic resistance from the electrolyte and interfacial polarizations from the electrodes. The large ohmic resistance can be decreased by reducing the electrolyte thickness and/or using alternative electrolyte materials such as doped ceria or doped lanthanum gallate that have much higher oxide-ion conductivities than the standard yttrium-stabilized zirconia (YSZ). Considering the dominant contribution of cathode to the overall interfacial polarizations, especially for the common anode-supported thin electrolyte SOFCs, development of novel cathode materials and microstructures with superior electrocatalytic activity and long-term stability are critically important to achieve high enough power density at reduced temperatures [6,7].

Perovskite oxides such as $La_{0.8}Sr_{0.2}FeO_{3-\delta}$, $Ba_{0.5}Sr_{0.5}Co_{0.8}Fe_{0.2}O_{3-\delta}$ and $Sm_{0.5}Sr_{0.5}CoO_{3-\delta}$ exhibit both electronic and ionic conductivities, and have been extensively investigated as the cathode materials for reduced-temperature SOFCs due to extension of the electrochemically

* Corresponding authors. Tel./fax: +86 21 6990 6373.
E-mail addresses: srwang@mail.sic.ac.cn (S. Wang), zzhan@mail.sic.ac.cn (Z. Zhan).

0378-7753/$ – see front matter © 2013 Elsevier B.V. All rights reserved.
http://dx.doi.org/10.1016/j.jpowsour.2013.07.113

reactive region from the traditionally triple-phase boundaries to the entire surface [8,9]. Recently, layered perovskite oxides with the $LnBaCo_2O_5$ formula have gained great interest as novel cathode materials because of their high oxygen surface exchange coefficients (k) and self-diffusion coefficients (D), *e.g.*, $D = 2.8 \times 10^{-10}$ cm^2 s^{-1} and $k = 7.5 \times 10^{-8}$ cm s^{-1} for $GdBaCo_2O_{5+x}$ at 500 °C [10,11], or $D = 3.6 \times 10^{-7}$ cm^2 s^{-1} and $k = 6.9 \times 10^{-5}$ cm s^{-1} for $PrBaCo_2O_{5+x}$ at 500 °C [12,13]. These values are substantially larger than what observed for most of common perovskite oxides, *e.g.*, $D = 3.9 \times 10^{-7}$ cm^2 s^{-1} and $k = 1.5 \times 10^{-10}$ cm s^{-1} for $La_{0.5}Sr_{0.5}CoO_3$ at 500 °C [14]. Tarancón explored the potential of $GdBaCo_2O_{5+x}$ as new cathode materials and reported a polarization resistance ($R_{P,C}$) value of 0.25 Ω cm^2 on $Gd_{0.1}Ce_{0.9}O_2$ (GDC) electrolytes at 650 °C [15]. $GdBaCoFeO_{5+x}$ (GBCF) was also investigated as cathode for intermediate-temperature solid oxide fuel cells and showed interfacial polarization resistances of 0.42, 0.18 and 0.11 Ω cm^2 at 550, 600 and 650 °C, respectively [16]. Recently, Zhou et al. showed that $SmBaCo_2O_{5+x}$ (SBCO) displayed good catalytic activity for oxygen reduction reactions [17], which can be further enhanced by partial substitution of Sr for Ba. In particular, $SmBa_{0.5}Sr_{0.5}Co_2O_5$ (SBSCO) exhibited interfacial polarization resistances of 1.01, 0.38, 0.16 and 0.06 Ω cm^2 at 500, 550, 600 and 650 °C [18]. Composites of SBSCO and GDC in a weight ratio of 1:1 showed even lower polarization resistances of 0.10 Ω cm^2 at 600 °C and 0.013 Ω cm^2 at 700 °C [19].

Reducing the feature size of cathode catalysts from the common micron scale down to the nano scale can accelerate oxygen reduction kinetics by providing enlarged number of active sites for surface oxygen exchange [20–22]. A cost-effective approach for obtaining nano-scale cathodes is to incorporate nanoparticles into the pre-formed porous backbones by impregnating appropriate solutions of soluble metal salts with the subsequent calcinations. Simple perovskite oxides such as doped $LaCoO_3$, $SmCoO_3$ and $LaFeO_3$ have been extensively used as the infiltration catalysts and have shown excellent performance as the cathodes for reduced-temperature SOFCs [23–25]. For example, the $Sm_{0.5}Sr_{0.5}CoO_3$ (SSC) infiltrated GDC composites show polarization resistances as low as 0.1 Ω cm^2 at 550 °C [24]. Even better performances, *e.g.*, 0.075 Ω cm^2 at 550 °C and 0.13 Ω cm^2 at 500 °C, were achieved by co-impregnating $Sm_{0.2}Ce_{0.8}O_{1.9}$ (SDC) in addition to SSC into the porous LSGM backbones [26]. Note that the $LnBaCo_2O_5$ layered perovskite system have rarely been used as the infiltration catalysts. In this work, nano-scale catalysts of $SmBa_{0.5}Sr_{0.5}Co_2O_5$ (SBSCO) were coated onto the pore walls of LSGM backbone and were evaluated as potential cathodes for reduced temperature SOFCs operating over the regime of 450–600 °C.

2. Experimental

Electrochemical properties of nano-scale SBSCO oxides as the active cathode catalysts were evaluated using symmetrical cathode fuel cells, which were based upon tri-layer structures of porous | dense | porous LSGM that were produced by laminating one dense LSGM tape and two porous LSGM tapes on both sides with subsequent co-firing at 1450 °C. Fig. 1 showed a typical fabrication process of both symmetrical cathode fuel cells and function fuel cells which used in this paper. To avoid the damage of electrolyte when hot pressing asymmetric function fuel cells, the pressure was set to be 800PSI, much lower than 3000PSI when fabricating symmetrical cathode fuel cells. The porous layers were filled with 40 wt% starch as the fugitive materials, yielding porosities of ≈40% as measured using the Archimedes'method. The SBSCO catalysts were added into the porous LSGM backbones by impregnating an appropriate precursor solution followed by calcinations at temperatures of 800–900 °C. The symmetrical cathode fuel cells were weighed before and after each impregnation–calcination cycle to estimate the loadings of impregnated SBSCO catalysts, which were expressed as the weight ratio of the impregnated oxides to the porous LSGM backbones plus impregnated oxides. A single impregnation/calcination cycle produced a SBSCO loading of 1.5–2 wt% in the porous LSGM backbone, so multiple impregnation/calcinations cycles were performed to increase the catalyst loadings. The precursor solutions were prepared as follows: stoichiometric amounts of the nitrate salts – $Sm(NO_3)_3 \cdot 6H_2O$, $Ba(NO_3)_2$, $Sr(NO_3)_2$ and $Co(NO_3)_3 \cdot 6H_2O$–were dissolved in distilled water. Citric acid was then added to the solution with the molar ratio of the citric acid to the total metal ions at 1.5:1. Ammonia was added to the above solution to adjust the PH value at ≈4 in order to ensure full chelation of citric acid with metal ions. The precursor solution was subsequently heated on a hot plate until a molar concentration of 0.5 mol L^{-1} was obtained. Electrochemical properties of impregnated SBSCO–LSGM composites were also evaluated on functional fuel cells, where only one side of porous LSGM backbones was coated with SBSCO catalysts while the other was impregnated with nickel nitrate solution with subsequent calcinations at 700 °C to form NiO. The typical NiO loadings were 21 wt%.

The phase compositions of the impregnated SBSCO–LSGM composites were examined using X-ray diffraction (XRD, Rigaku D/Max2500). XRD patterns were collected at room temperature with a step size of 0.02° in 2θ over the scanning range of 15–80°. The microstructure of the SBSCO–LSGM composites was examined using the field emission scanning electron microscope (FESEM-

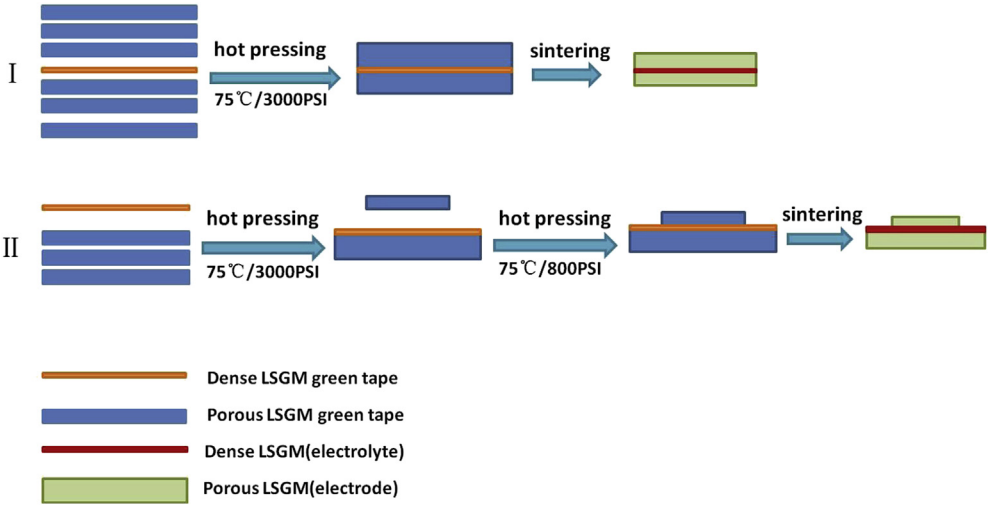

Fig. 1. A typical fabrication process of both (I) symmetrical cathode fuel cells and (II) function fuel cells which used in this paper.

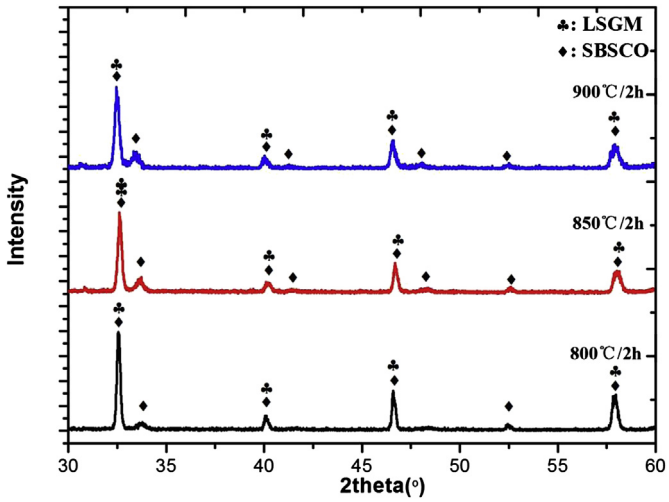

Fig. 2. Room temperature XRD patterns of SBSCO–LSGM composites calcinated at (a) 800, (b) 850 and (c) 900 °C.

4800). For electrochemical characterizations, silver inks were applied on the electrode surface and silver wires were used as the voltage and current leads. Impedance measurements of the symmetric cathode fuel cells, SBSCO–LSGM | LSGM | LSGM–SBSCO, were performed in the single chamber environment with the oxygen partial pressure ranging from 0.01 atm to 1 atm, using an IM6 Electrochemical Workstation (ZAHNER, Germany) with a frequency ranged from 0.1 Hz to 100 kHz with an amplitude of 20 mV. Impedance plots were fitted using the Zview software. The functional fuel cells were measured over 450–600 °C with humidified hydrogen fuels in the anodes and ambient air oxidants in the cathodes with a mass flow of hydrogen and air both 80 sccm. The measurement of conductivity of a homemade LSGM dense pellet was performed using a 4-probe DC Van der Pauw method.

3. Results and discussions

3.1. Structures and properties of the cathodes

Prior reports have shown that the layered perovskite oxides, $LnBaCo_2O_5$ (Ln = La, Pr, Nd, Sm, Gd), were chemically compatible with the LSGM electrolytes at temperatures below 1000 °C [15,17,27,28], and that partial substitution of Sr for Ba yielded better compatibility. For example, no chemical reaction was observed between the $GdBa_{1-x}Sr_xCo_2O_5$ cathodes and the LSGM electrolytes even at 1100 °C [28]. In the present work, infiltrates within the porous LSGM backbones were calcinated at 800–900 °C such that deleterious chemical reactions could be avoided. Room temperature X-ray diffraction patterns of the impregnated SBSCO–LSGM composites calcinated at 800, 850 and 900 °C are shown in Fig. 2, where relatively high loadings of 29 wt% were used to increase the diffraction peaks from infiltrates. In addition to large diffraction peaks from the LSGM backbones, some visible small peaks at 2θ = 34, 43 and 53 can be indexed to the layer perovskite SBSCO oxides. Increasing the calcination temperature yielded stronger diffraction peaks for SBSCO oxides, indicative of increased crystallization. Fig. 3 shows the representative SEM micrographs of the blank porous LSGM skeleton and impregnated SBSCO–LSGM

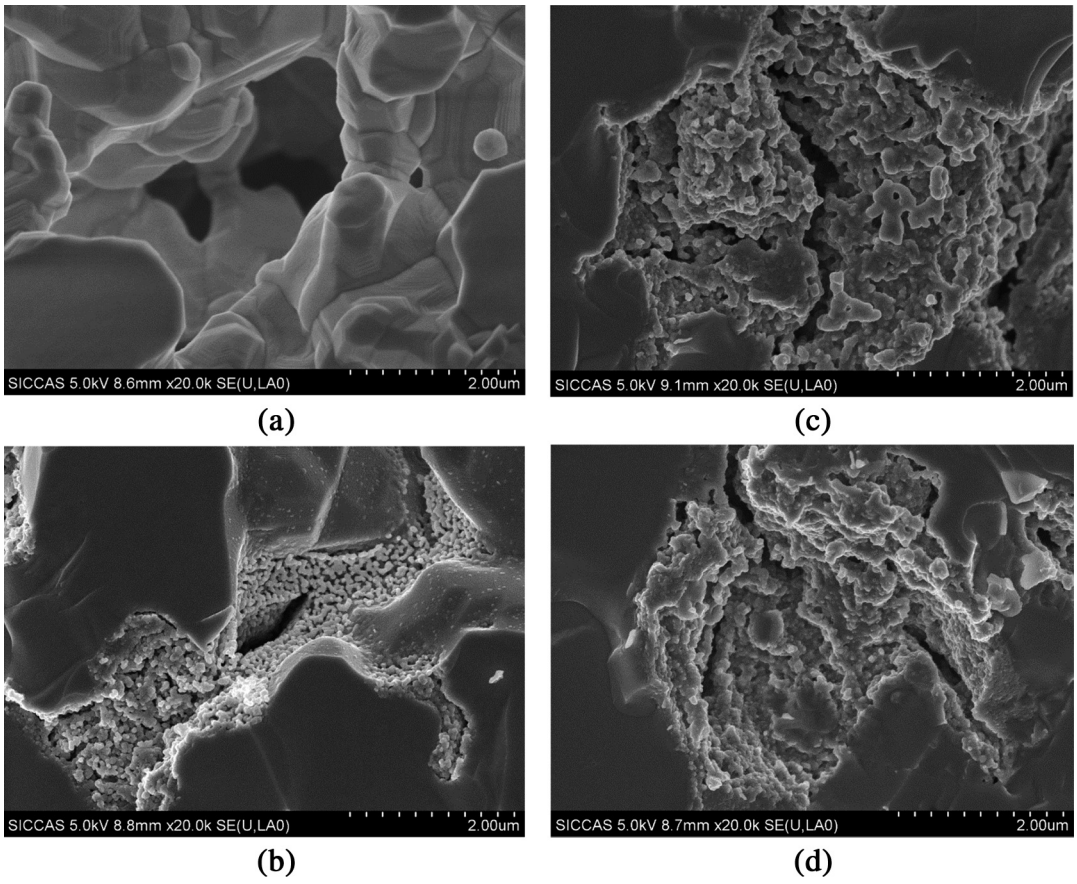

Fig. 3. The SEM micrograph of (a) the blank porous LSGM skeleton and SBSCO–LSGM composite cathodes calcinated at (b) 800, (c) 850 and (d) 900 °C.

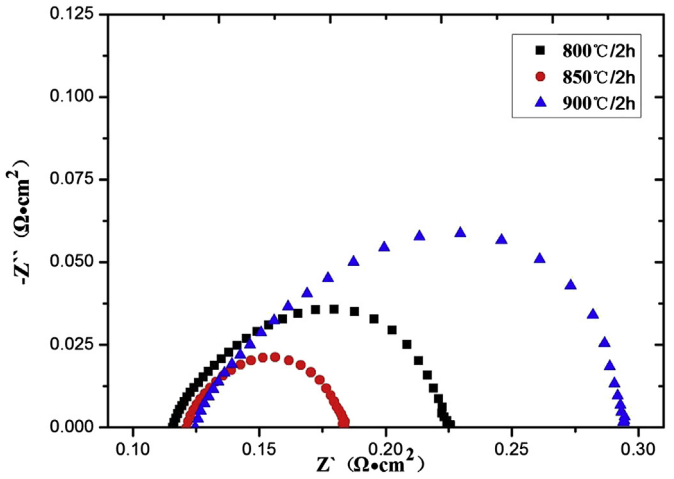

Fig. 4. Comparison of impedance data for symmetric SBSCO–LSGM cathode fuel cells with SBSCO catalysts calcinated at 800, 850 and 900 °C (the ohm resistance have been halved).

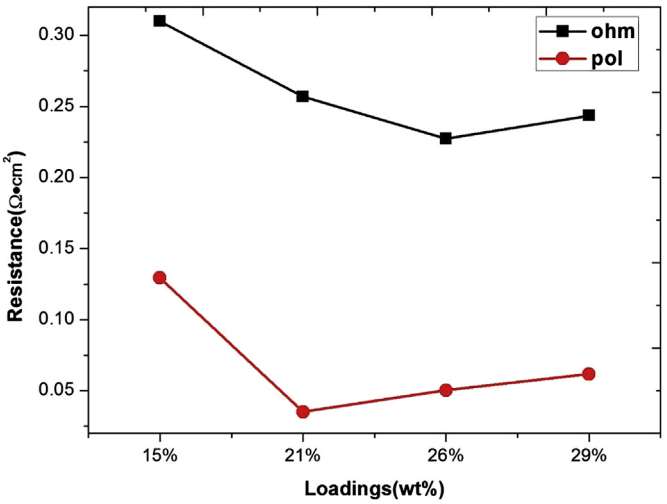

Fig. 6. The pure ohmic resistances (R_o) and the cathode polarization resistances ($R_{P,C}$), as obtained from impedance measurement of symmetric SBSCO–LSGM cathode fuel cells at 550 °C, plotted as a function of the SBSCO loadings.

composites calcinated at 800, 850 and 900 °C. For the composites calcinated at 800 °C, the LSGM backbones were covered with fine and well-interconnected coatings, and the typical tendril width for SBSCO catalysts was ≈80 nm. Increasing the calcination temperature resulted in more densely packed coatings and larger widths of the tendril SBSCO particles, *e.g.*, 175 nm at 850 °C and 350 nm at 900 °C.

Impedance measurements were conducted on symmetric cathode fuel cells to examine the influence of the calcination temperature on the catalytic activities of the impregnated SBSCO–LSGM composites for oxygen reduction reactions. Fig. 4 compares Nyquist plots of the impedance data as measured in air at 550 °C. The cathode polarization resistances ($R_{P,C}$), taken as the overall width of the depressed arcs in Nyquist plots, were 0.109, 0.057 and 0.125 Ω cm^2 for impregnated SBSCO–LSGM composites calcinated at 800, 850 and 900 °C respectively. The largest $R_{P,C}$ value for the sample calcinated at 900 °C can be explained by substantially reduced surface area available for oxygen reduction reactions due to excessive coarsening of SBSCO catalysts, as evidenced by large particle size shown in Fig. 3d. What is unexpected is that the sample calcinated at 800 °C consisted of SBSCO catalysts with the smallest particle size, but showed a polarization resistance that was approximately twice the value for the sample calcinated at 850 °C. One possible reason could be the presence of minor impurities in the infiltrates, which were difficult to be identified in the XRD patterns for the impregnated SBSCO–LSGM composites due to dominant peaks from the LSGM backbones. The SBSCO precursor solutions were gellated at 80 °C and then calcinated at 800, 850 and 900 °C, respectively. The X-ray diffraction patterns of the resulting powders are compared in Fig. 5 showing that phase-pure SBSCO oxides were only achieved after calcinated at 900 °C. For powders calcinated at 800 °C, the layered perovskite SBSCO oxide was the predominant phase, but appreciate amounts of impurity phases $Ba_{0.5}Sr_{0.5}CoO_3$ and $SrCoO_3$ were also observed, which might adversely influence the catalytic activity for oxygen reduction reactions. Despite the presence of minor impurities $SrCoO_3$, the SBSCO–LSGM composites calcinated at 850 °C showed the lowest cathode polarization resistances.

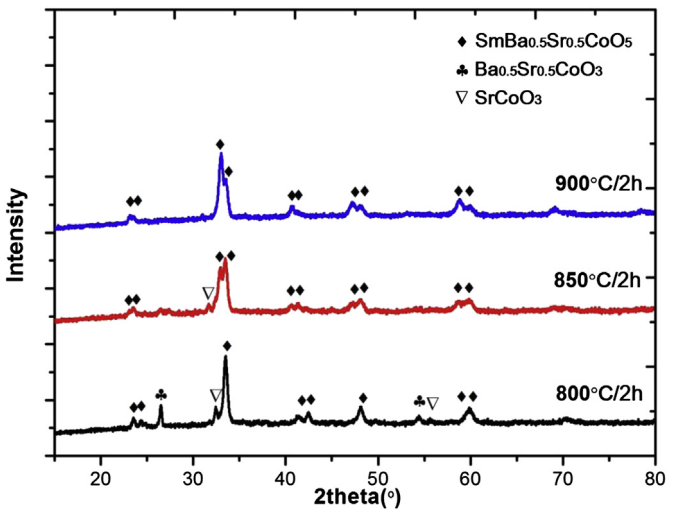

Fig. 5. Room temperature XRD patterns of SBSCO powders as obtained by calcination of the precursor solutions at (a) 800, (b) 850 and (c) 900 °C.

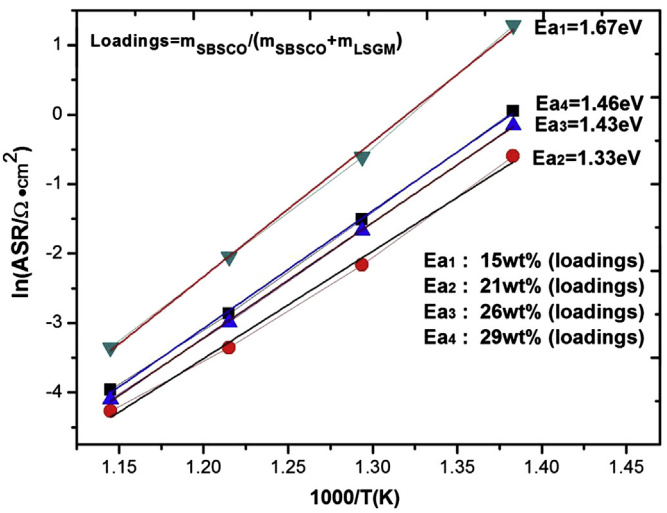

Fig. 7. The area special resistance as a function of temperature of SBSCO–LSGM composites fired at 850 °C at different loadings.

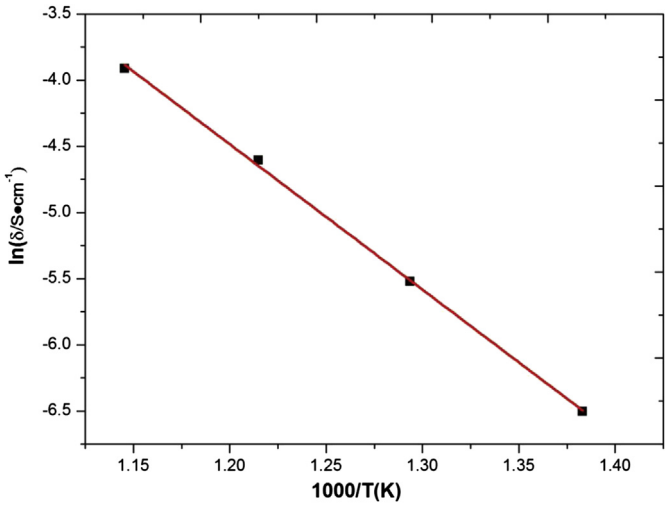

Fig. 8. Arrhenius plots of conductivity of a dense pellet of LSGM in the temperature range of 450–600 °C.

Note that the infiltrated catalysts play dual roles in the porous LSGM backbones – promoting oxygen reduction reactions that occur on their surfaces and collecting the electrical current. As shown in Fig. 3c–d, a solid loading of 29 wt% was sufficient to form catalyst coatings with high phase connectivity that was required to perform well as the electrocatalysts and the current collector. Attempts were also made to decrease the catalyst loading, such that the cathode porosity was increased and gas transport was facilitated. The cathode polarization resistances at varied SBSCO loadings are shown in Fig. 6, where all cathodes were calcinated at 850 °C. A minimum in the cathode polarization resistance was observed, *i.e.*, $R_{P,C} = 0.035\ \Omega\ cm^2$ at a SBSCO loading of 21 wt%. This is reasonable considering that reducing the SBSCO loading would increase the fraction of isolated catalyst particles that showed little catalytic activity for oxygen reduction reactions while increasing the SBSCO loading would reduce the cathode porosity and thereby increase the gas diffusion resistance. The area special resistance as a function of temperature of SBSCO–LSGM composites fired at 850 °C at different loadings was shown in Fig. 7. As can be observed that the 21 wt% SBSCO–LSGM composites calcinated at 850 °C showed the lowest activation energy, *e.g.*, 1.33 eV for 21 wt% while 1.67 eV for 15 wt% and 1.43 eV for 29 wt%. This corresponds very well with the results of EIS testing that the 21 wt% SBSCO–LSGM composites showed the lowest polarization. What is unexpected is that the optimum loadings of SBSCO was low compared with other literature. Such low optimum content of SBSCO may be related to the pore structure and(or) porosity of LSGM skeleton, though more research and evidence were needed. Considering that the range of SBSCO loading was not wide, further optimization is also needed, especially between 15 wt%–26 wt%. Anyway, the optimization is not our goal in this paper. For simplicity, 21 wt% SBSCO loadings was choose for our next study. Also summarized in Fig. 6 are the

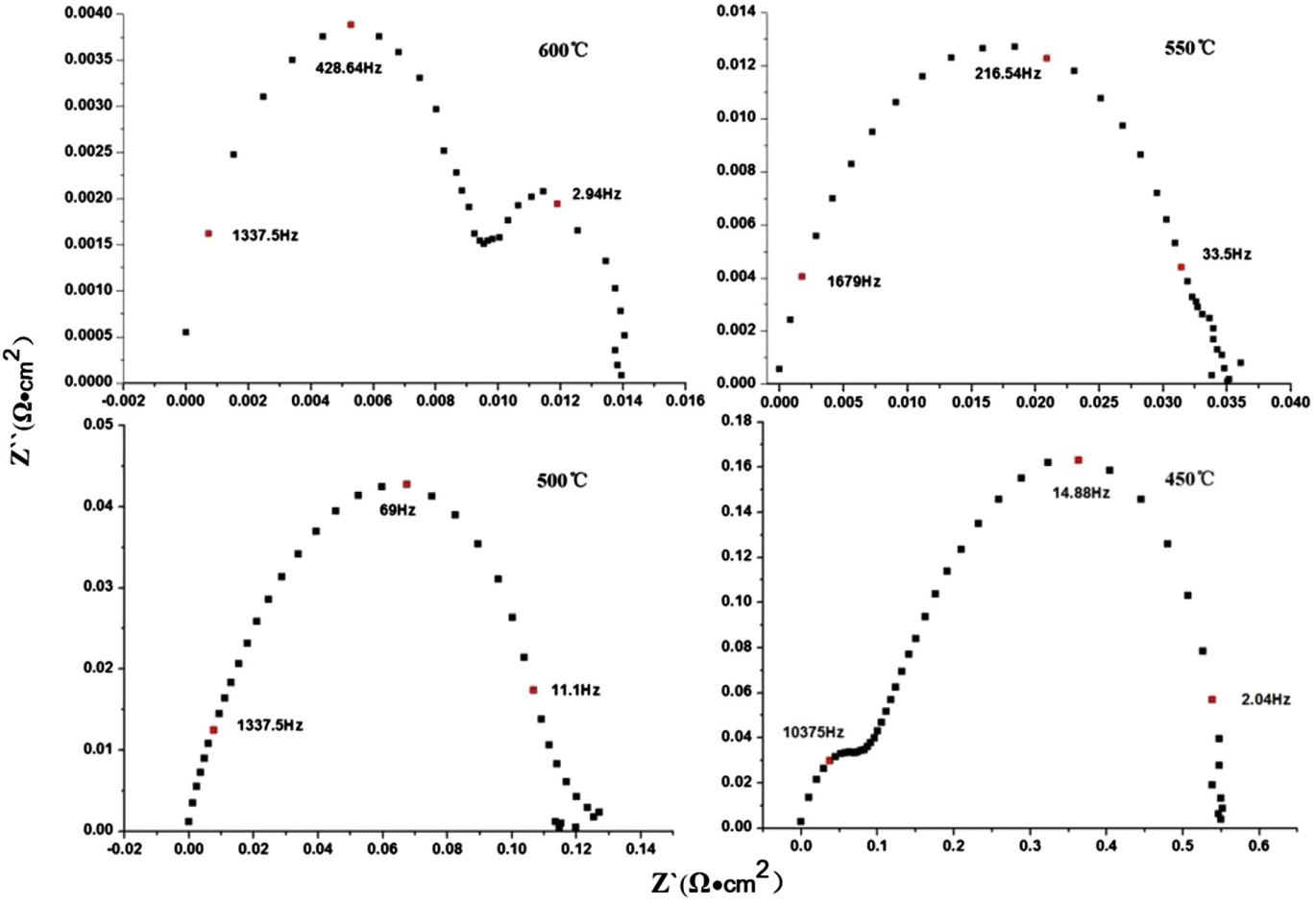

Fig. 9. Nyquist plots of the impedance data in air for symmetric SBSCO–LSGM cathode fuel cells with a SBSCO loading of 21 wt% at varied temperatures.

ohmic resistances (R_O) of the symmetric cathode fuel cells. The R_O value decreased from 0.31 Ω cm^2 at 15 wt% to 0.24 Ω cm^2 at 21 wt%, and tended to stable with further increasing SBSCO loading. These results suggest that the 21 wt% SBSCO–LSGM composites calcinated at 850 °C yielded the best cathode performance. Arrhenius plots of conductivity of dense pellet of LSGM was shown in Fig. 8 in the temperature range of 450–600 °C. As shown in Fig. 8, the conductivity of LSGM at 600, 550 °C, 500 °C and 450 °C was 0.02, 0.01, 0.004 and 0.0015S cm^{-1}. Note that the electrolyte was typically 19 μm, yielding an electrolyte resistance R_{EL} = 0.19 Ω cm^2 at 550 °C. The additional 0.05 Ω cm^2 can be due to contact resistances or current collection losses in the testing setup [29].

3.2. Oxygen reduction mechanism

Fig. 9 shows Nyquist plots of the impedance data measured in air for symmetric cathode fuel cells with 21 wt% SBSCO catalysts calcinated at 850 °C. The cathode polarization resistances were 0.013, 0.035, 0.12 and 0.55 Ω cm^2 at 600, 550, 500 and 450 °C, respectively. These values were substantially smaller than previously observed for micron-scale layered perovskite oxide cathodes, *e.g.*, 0.1 Ω cm^2 for SBSCO–GDC composites at 600 °C [19], 0.093 Ω cm^2 for $PrBa_{0.92}Co_2O_5$ at 600 °C [30], 0.25 Ω cm^2 for $GdBaCo_2O_{5+x}$ at 625 °C [15], 0.25 Ω cm^2 for $SmBa_{0.5}Sr_{0.5}Cu_2O_5$ at 650 °C [31], 0.25 Ω cm^2 for $NdBa_{0.5}Sr_{0.5}Co_2O_5$ at 700 °C and 0.11 Ω cm^2 for $NdBaCo_2O_5$ at 700 °C [32]. The present nano-scale SBSCO–LSGM composites also showed higher catalytic activities for oxygen reduction reactions than alternative nano-scale layered-perovskite oxides. For example, nanostructured $PrBaCo_2O_{5+x}$ cathodes showed a polarization resistance of 0.086 Ω cm^2 at 600 °C [33].

Comparison of these impedance spectra in Fig. 9 indicates that oxygen reduction reactions on the impregnated SBSCO–LSGM composite cathodes consisted of at least three different elementary steps with the relaxation frequencies at 10^4, 10 ~ 10^3 and 1–10 Hz (referred as high-, middle- and low-frequencies), respectively. The impedance spectra at 600 °C consisted of a large middle-frequency arc and a small low-frequency arc. With decreasing temperature down to 550 and 500 °C, the middle-frequency arc increased pronouncedly while the low-frequency arc gradually overlapped with the middle-frequency arc. Further reduction in temperature to 450 °C resulted in the appearance of the high-frequency arc in the Nyquist plot.

Alder et al. has shown that the high-frequency arc is related to charge transfer along the cathode|electrolyte interfaces with a characteristic frequency >10^4 Hz, while the middle- and low-frequency arcs are surface-dominated and might result from oxygen surface exchange, solid-state diffusion, or gas-phase diffusion inside and outside the electrode, which called chemical impedance associated with non-charge-transfer processes [34,35]. What is interesting is that the high-frequency arc was only evidenced in the low temperature region, *i.e.*, 600 °C showed by Adler et al. [35] and 450 °C in our research. Since the high-frequency resistance was negligibly small at temperatures above 450 °C, these impedance data were fitted using a simplified equivalent circuit schematically shown in Fig. 10, where R_m and R_l were the resistances while Q_m and Q_l were the constant phase elements for the middle- and low-frequency arcs, respectively. The resulting R_m and R_l values at

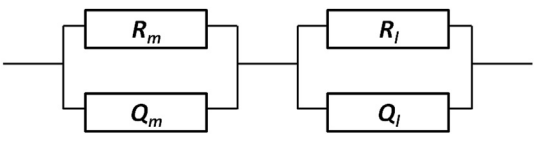

Fig. 10. The equivalent circuit for fitting of the impedance data.

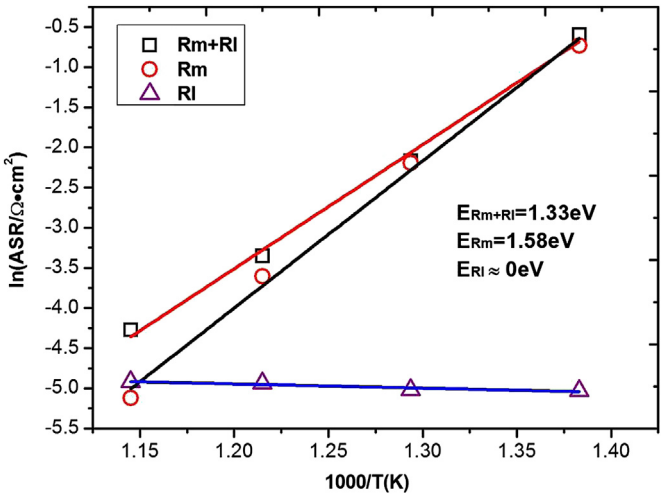

Fig. 11. Temperature dependence of the middle- and low-frequency arcs for impedance spectra shown in Fig. 9.

different temperatures are summarized in Fig. 11. The temperature independence of the low-frequency arc indicated that it might be related to oxygen transport or non-dissociative adsorption of oxygen molecules on the catalyst surfaces. In contrast, the middle-

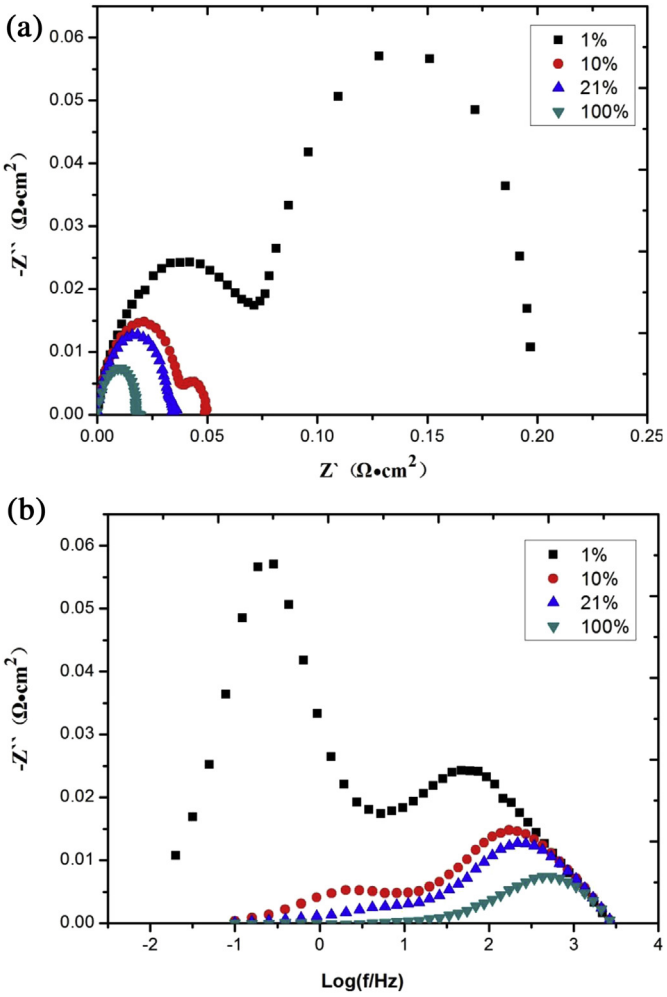

Fig. 12. (a) Nyquist and (b) Bode plots of impedance data for the symmetric fuel cells under varied oxygen partial pressures balanced by nitrogen.

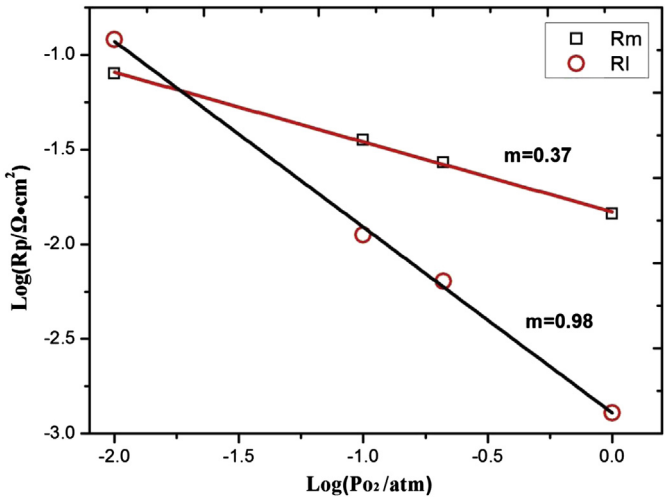

Fig. 13. Oxygen partial pressure dependence of the middle- and low-frequency arcs for impedance spectra shown in Fig. 12.

frequency arc followed an Arrehenius dependence with an activation energy of 1.58 eV.

Note that cathode polarization resistance usually decreases with increasing oxygen partial pressure and can be expressed as follows,

$$\frac{1}{R_p} \propto P_{O_2}^{m} \tag{1}$$

where the m value can provide some information on the rate-limiting step for oxygen reduction reactions [36], *e.g.*,

$$O_{2,gas} \leftrightarrow O_{2,ads} \quad m = 1 \tag{2}$$

$$O_{2,ads} \leftrightarrow 2O_{ads} \quad m = 1/2 \tag{3}$$

$$O_{ads} + e \leftrightarrow O_{ads}^{-} \quad m = 3/8 \tag{4}$$

$$O_{ads}^{-} + e \leftrightarrow O_{ads}^{2-} \quad m = 1/8 \tag{5}$$

Fig. 12a and b shows Bode and Nyquist plots for symmetric cathode fuel cells with 21 wt% SBSCO catalysts measured at 550 °C in homogeneous atmospheres with varied oxygen partial pressures. At oxygen partial pressure $P_{O_2} = 0.01$ atm, the Nyquist plot consisted of two distinct arcs, centered at the middle- and low-frequency frequencies, respectively. Both arc decreased pronouncedly with increasing oxygen pressure, and the low-frequency arc became overlapped with the middle-frequency arc for $P_{O_2} \geq 0.21$ atm. Similarly, these impedance data were also fitting using the equivalent circuit in Fig. 10 and the dependences of the resulted R_m and R_l values on oxygen partial pressure are shown in Fig. 13. The fitted m values were 0.37 for R_m and 0.98 for R_l, indicating that the middle- and low-frequency arc correspond respectively to ionization of adsorbed oxygen atom (step 4) and non-dissociative adsorption of oxygen molecules (step 1). The latter was also supported by the temperature independence of the lower-frequency arc, as shown in Fig. 11. Fig. 13 also shows that the R_m value in air was several orders of magnitude larger than the R_l value, suggesting oxygen reduction reactions were largely limited by ionization of adsorbed oxygen atom.

3.3. Single cell performances

The electrochemical properties of the impregnated SBSCO–LSGM cathodes were also examined on functional fuel cells that were also based upon the tri-layer structure of porous | dense | porous LSGM with one porous layer infiltrated with SBSCO oxides and the other with NiO. The LSGM electrolyte layer was also 19 μm thick, the same as symmetrical fuel cell. The typical schematic of our testing system was showed in Fig. 14. Such fuel cells were measured over the temperature range of 450–600 °C with humidified hydrogen in the anode and ambient air in the cathode, with plots of cell voltages and power densities versus current densities shown in Fig. 15a and Nyquist plots of impedance data at open circuits shown in Fig. 15b. The maximum power densities were 1.50, 1.18, 0.70 and 0.25 W cm^{-2} at 600, 550, 500 and 450 °C, respectively. The overall polarization resistances, including contributions from both the anode and the cathode, were 0.088, 0.127, 0.27 and 0.816 Ω cm^2 at 600, 550, 500 and 450 °C, respectively. Considering that the fabrication of symmetric cell and single cell is different, the polarization resistance of cathode obtained in symmetric cell and single cell is different. Prior research showed that the Ni impregnated LSGM composites exhibited excellent catalytic activities for hydrogen oxidation reactions and thereby enabled negligible polarization resistances, *e.g.*, 0.011 Ω cm^2 at 550 °C [37].

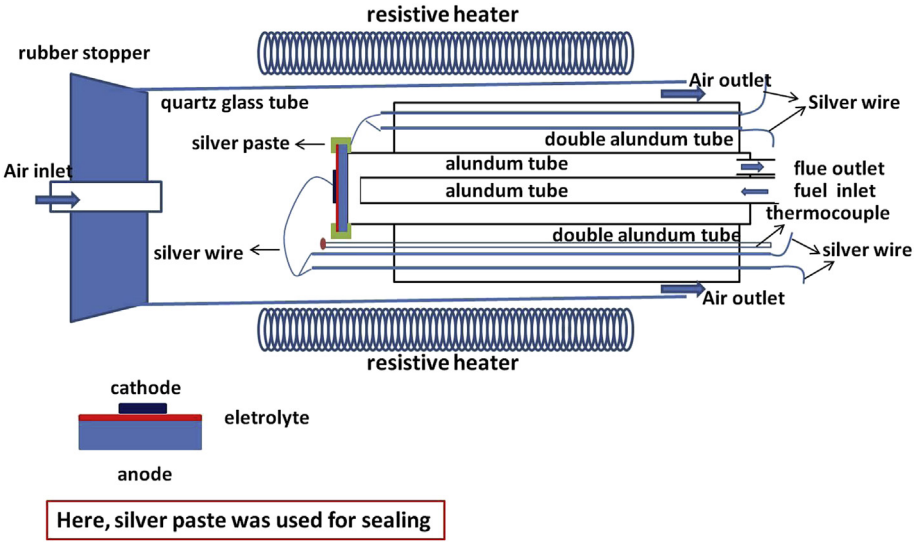

Fig. 14. A typical schematic of our testing system.

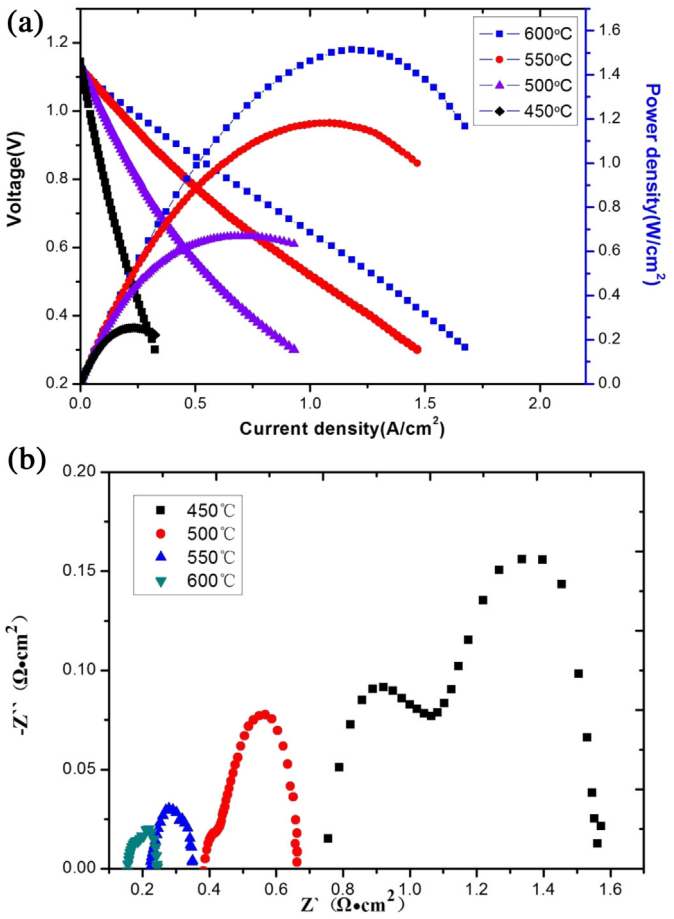

Fig. 15. (a) Cell voltages and power densities plotted versus current density at different temperatures for thin LSGM electrolyte fuel cells with impregnated SBSCO cathodes and Ni anodes, operating on 97% H_2 − 3% H_2O fuels and ambient air oxidants. (b). Nyquist plots of impedance data at open circuits at different temperatures for thin LSGM electrolyte fuel cells with impregnated SBSCO cathodes and Ni anodes, operating on 97% H_2 − 3% H_2O fuels and ambient air oxidants.

Therefore, superior performance of thin LSGM electrolyte fuel cells at reduced temperatures can be primarily ascribed to the excellent catalytic activities of the impregnated SBSCO–LSGM composites for oxygen reduction reactions.

4. Conclusions

We have fabricated the composite cathode by impregnating nano-scale SBSCO coatings into the porous LSGM backbones. Despite the presence of minor $SrCoO_3$ impurities, the catalysts calcinated at 850 °C exhibited the lowest polarization resistance in air, ranging from 0.013 Ω cm^2 at 600 °C to 0.12 Ω cm^2 at 500 °C. Thin LSGM electrolyte fuel cells with impregnated SBSCO cathodes and Ni anodes delivered maximum power densities of 1.50, 1.18, 0.70 and 0.25 W cm^{-2} at 600, 550, 500 and 450 °C, respectively. These results demonstrate great promise of the impregnated SBSCO–LSGM composites as the cathodes for reduced-temperature SOFCs operating at 450–600 °C. Impedance analysis indicates that oxygen reduction reactions for the impregnated SBSCO–LSGM composites in air were dominated by ionization of adsorbed oxygen atoms on the SBSCO catalyst surfaces.

Acknowledgments

The authors gratefully acknowledge the financial support of the National Basic Research Program of China under contract No. 2012CB215401, the National Science Foundation of China under contract No. 51072219, Science and Technology Commission of Shanghai Municipality under contract No. 11PJ1410300, Science and Technology Commission of Zhejiang Province under contract No. 2011C16037, and Chinese Government High Tech Developing Project under contract No. 2011AA050702.

References

[1] Toru Inagaki, Kazuhiro Miura, Takehisa Fukui, et al., J. Power Source 86 (2000) 347–351.
[2] Yu-Mi Kim, Su-Il Pyun, Ju-Sik Kim, Gyoung-Ja Lee, J. Electrochem. Soc. 154 (8) (2007) B802–B809.
[3] Yihong Li, Randall Gemmena, Xingbo Liua, J. Power Sources 195 (2010) 3345–3358.
[4] Allan J. Jacobson, Chem. Mater. 22 (2010) 660–674.
[5] Narottam P. Bansal, Zhimin Zhong, J. Power Sources 158 (2006) 148–153.
[6] Z.Q. Deng, J.P. Smit, H.J. Niu, G. Evans, M.R. Li, Z.L. Xu, J.B. Claridge, M.J. Rosseinsky, Chem. Mater. 21 (2009) 5154–5162.
[7] Ethan J. Crumlin, Sung-Jin Ahn, Dongkyu Lee, Eva Mutoro, Michael D. Biegalski, Hans M. Christen, Yang Shao-Horn, J. Electrochem. Soc. 159 (7) (2012) F219–F225.
[8] Baoming An, Wei Zhou, Youmin Guo, Ran Ran, Zongping Shao, Int. J. Hydrogen Energy 35 (2010) 5601–5610.
[9] F. Mauvy, J.-M. Bassat, E. Boehm, J.-P. Manaud, P. Dordor, J.-C. Grenier, Solid State Ionics 158 (2003) 17–28.
[10] Albert Taranco'n, et al., J. Mater. Chem. 17 (2007) 3175–3181.
[11] A. Taranco, et al., Solid State Ionics 179 (2008) 611–618.
[12] G. Kim, S. Wang, A.J. Jacobson, Z. Yuan, W. Donner, et al., Appl. Phys. Lett. 88 (2006) 024103.
[13] G. Kim, C.A. Mims, et al., J. Mater. Chem. 17 (2007) 2500–2505.
[14] F. Mauvy, et al., J. Eur. Ceram. Soc. 24 (2004) 1265–1269.
[15] A. Tarancón, et al., Solid State Ionics 179 (2008) 2372–2378.
[16] Hanping Ding, Xingjian Xue, Int. J. Hydrogen Energy 35 (2010) 4316–4319.
[17] Qingjun Zhou, Tianmin He, J. Power Sources 185 (2008) 754–758.
[18] Hanping Ding, J. Power Sources 194 (2009) 815–817.
[19] Jung Hyun Kim, Joongmyeon Bae, et al., Chem. Mater. 22 (2010) 883–892.
[20] Xiaoyuan Lou, et al., J. Power Sources 195 (2010) 419–424.
[21] John M. Vohs, Raymond J. Gorte, Adv. Mater. 21 (2009) 943–956.
[22] San Ping Jiang, Int. J. Hydrogen Energy 37 (2012) 449–470.
[23] Jing Chen, Jian Li, et al., J. Power Sources 183 (2008) 586–589.
[24] Fei Zhao, Fanglin Chen, et al., J. Power Sources 185 (2008) 13–18.
[25] Yingyi Huang, John M. Vohs, Raymond J. Gorte, J. Electrochem. Soc. 151 (4) (2004) A646–A651.
[26] Zhongliang Zhan, Da Han, Scott A. Barnett, et al., RSC Adv. (2012) 1–4.
[27] J. Peña-Martínez, A. Tarancón, P. Núñez, Fuel Cells 08 (5) (2008) 351–359.
[28] J.-H. Kim, F. Prado, A. Manthiram, J. Electrochem. Soc. 155 (10) (2008) B1023–B1028.
[29] Da Han, Xuejiao Liu, Fanrong Zeng, Jiqin Qian, Tianzhi Wu, Zhongliang Zhan, Sci. Rep. 2, 462.
[30] Shengli Pang, et al., Int. J. Hydrogen Energy 37 (2012) 3998–4001.
[31] Xifeng Ding, Yujie Zhong, et al., Int. J. Hydrogen Energy 37 (2012) 2546–2551.
[32] Jung Hyun Kim, et al., Int. J. Hydrogen Energy 37 (2012) 5920–5929.
[33] Yao Wang, Han Zhang, Fanglin Chen, Changrong Xia, J. Power Sources 203 (2012) 34–41.
[34] S.B. Adler, Solid State Ionics 111 (1998) 125–134.
[35] S.B. Adler, J.A. Lane, B.C.H. Steele, J. Electrochem. Soc. 144 (5) (May 1997).
[36] Zhan Gao, Xingmin Liu, Bill Bergman, Zhe Zhao, J. Power Sources 196 (2011) 9195–9203.
[37] Xuejiao Liu, Xie Meng, Da Han, Hao Wu, Fanrong Zeng, Zhongliang Zhan, J. Power Sources 222 (2013) 92–96.